ACS APPLIED NANO MATERIALS

www.acsanm.org Article

Liquid Crystal Films as Active Substrates for Nanoparticle Control

Ines Gharbi, Viviana Palacio-Betancur, Habib Ayeb, Dominique Demaille, Juan J. de Pablo, Randall D. Kamien, and Emmanuelle Lacaze*

Cite This: *ACS Appl. Nano Mater.* 2021, 4, 6700−6708 Read Online

ACCESS | Metrics & More | Article Recommendations | Supporting Information

ABSTRACT: Organizing nanoparticles in a controlled way allows us to monitor their optical properties. It is particularly interesting to organize them on top of liquid crystal films to take advantage, in a second step, of the easy actuation of liquid crystals with external parameters such as temperature, electric fields, and so forth. We show that despite their fluidity, nematic and smectic films allow the formation of well-ordered hexagonal domains of gold spherical nanoparticles (AuNPs) at their surface, but we also show that both nematic films and AuNP domains impact each other. Using optical microscopy, atomic force microscopy (AFM), scanning electron microscopy (SEM), and spectrophotometry, we compare nematic, polymer-stabilized nematic, and smectic films with AuNP domains made of NPs of diameter 6 nm. On the liquid crystal films, depressions are revealed below the AuNP domains, whereas the AuNP domains appear well-organized but with a hexagonal period shortened with respect to AuNP monolayers formed on hard substrates. We interpret these features by the anchoring tilt imposed by the AuNP domains on the liquid crystal molecules. The smectic-A layers characteristic of the nematic surface transform into smectic-C layers, which induce the formation of depression. The energy penalty associated with the local smectic-A/smectic-C transition induces the shortening of the AuNP domain period in order to decrease the AuNP domain surface. The observed large depth of the polymer-stabilized nematic depressions below AuNP domains may be explained either by an increased size of the polymer-stabilized smectic layers close to the surface or by an increased number of polymer-stabilized smectic liquid crystal smectic layers close to the surface with respect to pure nematic films.

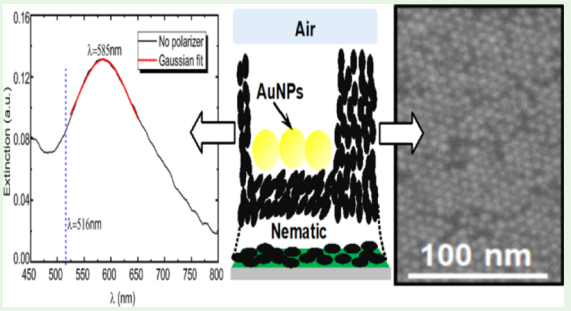

KEYWORDS: *liquid crystal, gold nanoparticle, nanoparticle control, plasmon extinction, spectrophotometry, AFM, SEM*

Liquid crystals (LCs) are the original nanomaterials: subjugated by surface forces, electromagnetic fields, and flow, they can be organized, actuated, and switched while maintaining sub-micron order. When combined with nanoparticles (NPs), these composites become of interest for applications[1,2] either to induce a modification of LC properties in the presence of NPs[3−7] or to allow for controlled NP organization mediated by the LC matrix. These last applications rely on the anisotropy of the LC matrix and its ease of manipulation through external stimuli (temperature or electric field) to build NP clusters that can be modified on demand by these external stimuli.[8] Commonly, NPs aggregate in a LC bulk without a particular ordering.[9,10] One alternative to engineer ordered NP structures is using topological defects, regions with mismatching LC molecular orientation, as sites for adsorbing NPs.[11−15] As a result, topological defects can be used as templates for the formation of NP clusters with supramolecular order.[16−19]

However, forming NP−LC composites through defect engineering is a challenging task since not only does it require the formation of well-defined topological defect arrays but also it is limited to NP sizes small enough to match the topological defect core sizes and surface chemistries that stabilize the defect morphology of interest. Efforts to use a LC matrix with a low density of defects as a substrate for NP self-assembly at the LC surface without the formation of uncontrolled clusters are therefore another interesting challenge. It has been reported that a cholesteric LC film, with a molecular pitch of the order of microns, exhibits a fingerprint texture which guides the NPs into ribbon-like assemblies, revealing the presence of more favorable areas at the surface of these modulated LC matrices.[20−24] However, a deep study of the local NP structure that drives the NP optical properties, in particular the light absorption when plasmonic NPs are concerned, and its relationship with the LC matrix specificity, is still lacking.

In this work, we demonstrate the stabilization of large collections of spherical gold nanoparticles (AuNP) domains on top of defect-free 5CB nematic and polymer-stabilized 5CB

Received: March 9, 2021
Accepted: May 20, 2021
Published: June 21, 2021

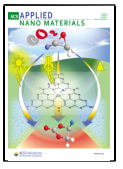

https://doi.org/10.1021/acsanm.1c00680
ACS Appl. Nano Mater. 2021, 4, 6700−6708

nematic films. These domains exhibit hexagonal packing, similar to ordered domains of particles on hard substrates. The presence of NP domains alters the topography of the free-standing 5CB film, while the inter-AuNP distance between AuNPs is shortened and thus red-shifts the plasmonic wavelength associated with AuNP light absorption. We show that similar phenomena are induced at the surface of free-standing 8CB smectic-A films and interpret these mutual modifications as arising from the AuNP-induced variation of anchoring at the interface.

MATERIALS AND METHODS

Solid Substrate Preparation. Polyvinyl alcohol (PVA) was spin-coated onto clean glass slides, baked for at least 1 h at 120 °C to polymerize, and rubbed unidirectionally with a commercial rubbing cloth to promote planar anchoring at the surface. This treatment is used on glass slides for nematic liquid crystal (NLC) and polymer-stabilized nematic liquid crystal (PSNLC) samples; on the silicon (SI) substrate to visualize the AuNPs without the LC; on glass slides coated with a thin transparent layer of indium thin oxide (ITO) to visualize PSNLC samples by SEM.

Photopolymerizable Monomer−NLC Mixture. In order to obtain PSNLC films, 4-pentyl-4′-cyanobiphenyl (5CB, Sigma-Aldrich—Figure 1a) was mixed with RM257 (30 wt %, Synthon

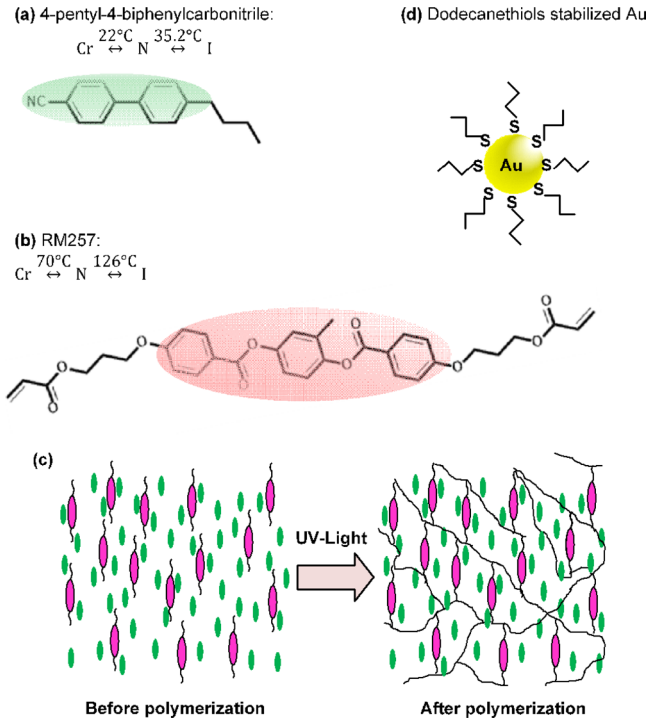

Figure 1. Chemical structures of (a) 5CB and (b) RM257. (c) Schematic presentation of the polymerization by UV irradiation of the reactive monomers RM257 to form PSNLC films. RM257 are represented in pink; 5CB are represented in green. (d) AuNP of diameter 6 nm.

Chemicals GmbH & Co. KG—Figure 1b) and a photo-initiator (1-hydroxycyclohexylphenylketone, 1,2 wt %, Sigma-Aldrich). To ensure better miscibility, dichloromethane is added. The LC monomer mixture is heated in a closed flask at 60 °C for 45 min, during which dichlormethane is in the gaseous phase. Once homogeneous, the flask is opened and all dichloromethane evaporates.

AuNP Synthesis. 1,2,3,4-Tetrahydronaphthalene (tetralin, 99% Aldrich), chlorotriphenylphosphine Au (I) (98%), and tert-butylamine borane (97%) were obtained from STEM Chemicals. Dodecanethiol (DDT), oleylamine, HAuCl4 (98%), and hexane were obtained from Sigma-Aldrich and toluene (98%) from Riedel de Haen. Ethanol (99.85%) and chloroform (99.2%) were from VWR. All reagents were used as received without further purification. The synthesis is based on ref 25; 50 mg of HauCl4 is mixed in a three-neck flask with 5 mL of oleylamine and 5 mL of tetralin and degassed at room temperature. The flask is dipped in an ice bath. The temperature controller is put in the ice bath rather than in the three-neck flask. Meanwhile, 22 mg of tertbutylborane is mixed with 0.5 mL of oleylamine and 0.5 mL of tetralin. The mixture is sonicated until full dissolution of the salt. The three-neck flask is put under Ar. The borane solution is injected promptly. The solution changes color to brown and then to purple. The reaction is continued for 36 min. 0.5 mL of DDT is added to stop the reaction growth. The content of the flask is mixed with 5 mL of ethanol and then centrifuged. The formed pellet is redispersed in toluene. NPs of diameter D = 6 nm surrounded by DDT ligands (Figure 1d) and polydispersity of 9% were obtained as shown by SAXS measurements performed on synchrotron Soleil.

NLC and PSNLC Film Preparation with or without AuNPs. Once the PVA-coated glass is prepared, 10 μL of the nematic material is spin-coated (2000 rpm for 20 s) to achieve uniform thickness throughout the film. This effectively generates a hybrid film, with planar anchoring on the PVA substrate and homeotropic anchoring at the nematic−air interface. The uniformity in thickness is checked by optical microscopy and profilometer measurements. The AuNP solution (with a concentration of 5.6×10^{17} AuNPs/L) is deposited by drop casting on the nematic film. Evaporation of the solvent can either induce contraction of the LC film or division into two or three smaller films, depending on the solvent evaporation. In a second step, to induce polymerization (Figure 1c), the samples were irradiated in a nitrogen atmosphere with a UV light of 0.15 mW cm^{-2} intensity at wavelength 365 nm for 20 min at room temperature.[26,27]

Smectic LC Film Preparation with AuNPs. Homeotropic substrates were prepared by spin-coating 50 μL of a 0.1 wt % DMOAP solution on clean glass and they were baked at 100 °C for 1 h. Hexagonal Cu grids were placed on the substrate to ensure uniform thickness and that a uniform homeotropic smectic film is formed.[28] The LC, in this case 8CB, purchased from Sigma-Aldrich, was heated above its clearing temperature and deposited on the grids. The film cools down and at room temperature forms a smectic phase. Optical microscopy images were taken to confirm a homeotropic film was formed. To deposit AuNPs on the smectic film, a 10 μL solution of AuNPs and toluene is deposited 1 μL at a time, and enough time is given to allow the toluene to evaporate.

Sample Characterization. *Polarized Optical Microscopy (POM).* The manufactured films are visualized using a LEICA DMRX microscope surmounted by a SONY CCD camera. A xenon lamp illuminates the sample in white light, placed so that the rubbing direction is oriented at 45° from the polarizer and the analyzer. This position allows us to have the maximum intensity.

Atomic Force Microscopy. Atomic force microscopy (AFM) images were obtained on PSNLC films and on smectic films with and without AuNPs using a Veeco model Nanoscope Dimension 3100 and a 500 kHz cantilever/stylus in the tapping mode.

Scanning Electron Microscopy. Scanning electron microscopy (SEM) images were obtained on PSNLC films with AuNPs using a ZEISS scanning electron microscope.

Spectrophotometry. The extinction spectra for spherical isolated AuNPs in toluene were measured using a Cary 5000 UV−vis−near-infrared spectrophotometer. The experimental data were fitted with a Gaussian curve. Spectra for the AuNPs of 6 nm diameter display a plasmon resonance of 516 nm (Supporting Information Figure S3).

A Maya 2000 Pro micro spectrophotometer coupled to a Leica optical microscope through an optical fiber was used to measure the light absorption of PSNLC−AuNP and NLC samples. The sample was illuminated by a white light source, and areas of 150 μm × 150 μm are probed with a 50× objective lens. All spectra were taken at room temperature in the 190−1100 nm spectral range. A reference

https://doi.org/10.1021/acsanm.1c00680
ACS Appl. Nano Mater. 2021, 4, 6700−6708

made of PSNLC (or NLC) of similar thickness but without AuNPs was used to extract the optical absorption of AuNPs only.

The distance between AuNPs was extracted from the extinction spectra using a dipole coupling model in the quasistatic approximation (NP diameter $D \ll$ wavelength λ).[29] In this approximation, the multipolar interactions between AuNPs as well as the retardance effect are not considered, this latter assumption being obviously correct due to the small size of AuNPs. In this case, the resonance condition can be calculated using the expression of the effective polarizability of an infinite AuNP hexagonal monolayer

$$\alpha_{\text{eff}} = \alpha/[1-\alpha\Sigma/4\pi(D+s)3] \quad (1)$$

with $\alpha = 4\pi(D/2)^3\ (\varepsilon - \varepsilon_m)/(\varepsilon + 2\varepsilon_m)$ being the polarizability of a single AuNP, so that the plasmonic resonance to the following equation[29]

$$\varepsilon = \varepsilon_m[\Sigma + 8(s/D+1)3]/[\Sigma - 4(s/D+1)3] \quad (2)$$

that relates ε the AuNP dielectric function, ε_m the dielectric function of the homogeneous surrounding, s the inter-AuNP gap in the hexagonal network, and D the AuNP diameter (D = 6 nm). Σ is the lattice sum associated with the AuNP assembly, AuNPs being considered as periodic dipoles. For monolayers considered as an infinite hexagonal network, the sum Σ is $\Sigma \approx 5.5$.[30,31]

The AuNP dielectric function was recalculated based on Johnson and Christy data[32] to take into account the small size effect and the influence of the chemical interface, leading to broadening and blue-shifted localized surface plasmon resonance of the isolated NPs in toluene.[33] ε_m is taken as equal to 2.28, previously shown to be mostly induced by the dodecanethiol ligands for these same AuNPs.[20]

RESULTS

Optical Microscopy Observations. 5CB Nematic films (Figure 1a) and polymer-stabilized 5CB nematic films (Figure 1b,c) on rubbed PVA substrates were prepared according to "Materials and Methods" section. In the following, we will refer to the polymer-stabilized 5CB nematic films as PSNLC and the 5CB nematic films as NLC. The nematic texture of PSNLC and of NLC, with and without gold spherical nanoparticles (AuNPs—Figure 1d), was first investigated by optical microscopy between crossed polarizers (POM) in transmission. The textures of the NLC and of the PSNLC appear similar (comparison between Figure 2a and between Figure 2b and Supporting Information Figure S1). For stability purposes, the results presented here are from PSNLC films unless indicated otherwise.

Profilometer measurements show that the thinnest section of the film is at the border, with a thickness of 6 μm, and the thickest region is at the center, with a thickness of 18 μm. These values correspond to the color of the optical microscopy pictures between crossed polarizers observed in Figure 2a for the NLC film, assuming that a hybrid film (planar anchoring on the rubbed PVA substrate and homeotropic anchoring in air) of LC has an effective birefringence of $\Delta\bar{n}_{LC} = n_{\text{eff}} - n_o$ with n_o, the ordinary LC index and n_{eff}, the effective extraordinary index determined by the following equation[34]

$$n_{\text{eff}} = \frac{1}{e}\int_0^e \frac{n_o n_e}{\sqrt{n_e^2\cos^2\theta(z) + n_o^2\sin^2\theta(z)}}\mathrm{d}z \quad (3)$$

with e the overall thickness, $\theta(z)$ the molecular orientation throughout the LC film (the director profile), and n_e and n_o the extraordinary and ordinary 5CB indexes. Minimizing the elastic energy gives $\theta(z)$ a linear profile subject to the boundary conditions.

For homeotropic anchoring in air, using n_o = 1.537 and n_e = 1.735, it can be calculated that $\Delta\bar{n}_{LC}$ is of the order of 0.1.[35] It decreased by 0.09 with respect to the nominal 5CB birefringence ($n_e - n_o$) = 0.19. The birefringence of monomer RM257 (with n_o = 1.508 and n_e = 1.687)[36] and that of 5CB are of the same order and we do not expect the polymer birefringence to significantly modify the PSNLC one.

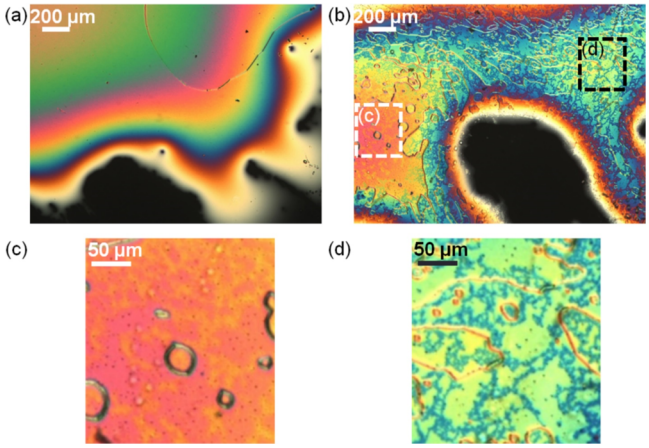

Figure 2. POM images in transmission between crossed polarizers where the molecules are aligned at 45° to the polarizer: (a) NLC film showing a color variation that corresponds to a thickness variation from the edge to the center of the film from 6 to 18 μm. (b) PSNLC film in the presence of AuNPs forming colored filament-like structures. (c) Enlarged view of AuNP yellow structures on a red nematic area. (d) Enlarged view of AuNP blue structures on a yellow nematic area.

On top of the NLC and the PSNLC, droplets of gold spherical nanoparticles (AuNPs of diameter 6 nm and covered by dodecanethiol ligands—Figure 1d) in toluene have been deposited. For PSNLC with AuNPs, the polymerization occurred after AuNP deposition. Large filaments or cluster structures are observed as shown in Figure 2b (for AuNP structures on the NLC film, see Supporting Information Figure S1). The difference between Figure 2a,b suggests that these domains are composed of AuNPs and the change in color indicates that their presence modifies the structure of the LC film underneath.

Figure 2c,d shows a magnified area of the PSNLC−AuNP films, where the areas with NPs appear blue-shifted. For example, the free nematic in red changes to yellow, and the free nematic in yellow changes to blue. This blue shift is systematic but can be more or less visible depending on the LC thickness and most probably also on the size and density of the NP domains. We might attribute this blue shift to two main phenomena: the domains of AuNPs form depressed regions on the PSNLC film altering its thickness, or the AuNPs impose a change of birefringence in the film. The observation of a large and well-visible blue shift of POM colors in the presence of AuNPs would imply non-negligible thickness changes with respect to the overall film thickness so that the second phenomenon is more likely to occur. In order to study the localization and organization of AuNPs in the domains identified by POM and to understand the origin of the local birefringence changes, we have studied PSNLC films with AuNPs using AFM.

AFM Measurements. Figure 3 shows that the macroscopic filament-like shape of the AuNP domains shown in Figure 2 is recovered on the AFM image through a contrast associated with variations in height (Figure 3a) and variations in phase (Figure 3b). AFM results reveal that, more locally, the

https://doi.org/10.1021/acsanm.1c00680
ACS Appl. Nano Mater. 2021, 4, 6700−6708

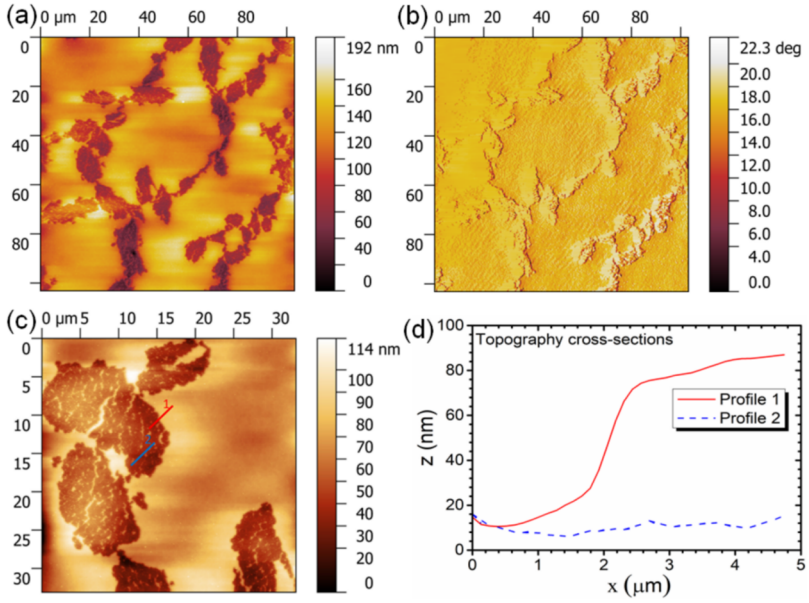

Figure 3. (a) AFM topographical and (b) phase data corresponding to the surface of a PSNLC film in the presence of AuNP domains. AuNP regions are visible in the phase data by the variations of phase contrast associated with variations of AFM tip interactions with the surface, which coincide with the zones of holes observed in (a). (c) Enlarged topographical view on the domains formed by AuNPs, revealing the formation of well-defined depressions at the nematic surface in the presence of AuNPs. (d) Topographical cross sections according to the lines drawn on (c). The depth of the hole formed by the AuNP domains is 60 nm with respect to the nematic surface. The bottom of the depression is flat.

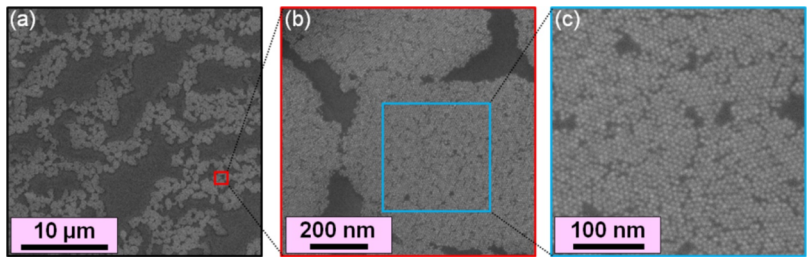

Figure 4. SEM images of the PSNLC−AuNP sample prepared in the same conditions as the one for spectrophotometry measurements and deposited on a conducting ITO substrate covered by rubbed PVA; (a) large-scale picture where AuNP domains appear as large AuNP filaments; (b) enlarged view of the structure showing associations of several domains which correspond to alternating areas with and without AuNPs, already seen by AFM. (c) Enlarged view inside the AuNP domain revealing an organization of AuNPs into well-ordered hexagonal monolayers.

filaments are divided into islands which are precisely visualized in Figure 3c. The comparison between POM and AFM pictures allows us to identify the islands as associated with the AuNP domains. The topography within the AuNP domains and on the free LC film is uniform as shown in Figure 3c,d. The AFM phase variation between the two regions, see Figure 3b, is related to different AFM tip/surface interactions. The observation of such an AFM phase variation demonstrates that the islands are made of AuNP domains localized at the LC surface and not covered in nematic material. It is however not possible to identify the nature of the AuNP packing within the domains given the limited AFM resolution. The change in thickness between the two zones, see Figure 3c,d, shows that the presence of AuNPs organized in domains impacts the nematic structure through the formation of depressions on the PSNLC film surface.

The depth of the islands relative to the PSNLC−air interface, Δe_{N-Au}, has been determined through 102 measurements performed on three samples. It varies between 20 and 100 nm with an average value $\Delta e_{N-Au} = 82 \pm 24$ nm. This Δe_{N-Au} value is, indeed, negligible compared to the thickness of the film (between 6 and 18 μm), which confirms that the color variation in Figure 2b−d is caused by a change in the birefringence. This birefringence change must be caused by the AuNP domains replacing air at the nematic surface. A layer of AuNPs of diameter 10 nm cannot significantly alter the birefringence of a nematic film of overall thickness between 6 and 18 μm. This increase of birefringence suggests that the antagonistic boundary conditions of a hybrid film are altered by the presence of the AuNP domains. It is no more perfectly homeotropic, as it was the case in the PSNLC−air interface, but becomes tilted.

The birefringence change can be estimated according to the following formula

$$\Delta\bar{n} = k\frac{\Delta\lambda}{e} \tag{4}$$

where $\Delta\bar{n}$ is the variation of birefringence with respect to $\Delta\bar{n}_{LC}$, k is the optical order, $\Delta\lambda$ is the difference in wavelength between the zones with and without AuNPs identified in the POM pictures, and e is the overall thickness. For the region between yellow and blue (Figure 2d), $\Delta\lambda$ is of the order of 100 nm and $k = 2$. Solving eq 4 for $\Delta\bar{n}$, the change in birefringence should be about 0.02. We calculate n_{eff} as a function of the

https://doi.org/10.1021/acsanm.1c00680
ACS Appl. Nano Mater. 2021, 4, 6700−6708

molecular orientation throughout the LC film. First, we assume that the director profile (the average LC molecule orientation) follows the analytical solution for a hybrid film described in eq 3. In such a case, a numerical solution for eq 3 yields an angle $\theta_1 = 17°$ if Δn is increased by 0.02 with respect to homeotropic anchoring at the surface. Second, if we assume that the texture in the areas with nanoparticles matches the adjacent texture in the areas without nanoparticles from the PVA ($\theta = 90°$) up until some tilt angle θ_2 and then remains at that constant angle all the way to the AuNP interfaces, we find that $\theta_2 = 39°$ for an increase Δn of 0.02. This appears to be the maximum LC tilt below the AuNP domains, consistent with the observed birefringence. Such tilted anchoring appears consistent with previous results of the literature since the dodecanethiol ligands grafted on an Au surface can induce tilted anchoring for short enough alkyl chains.[37]

SEM Investigations. POM and AFM pictures show how AuNPs impact a nematic film, once deposited at the surface. A change of anchoring is induced below the AuNP domains that form at the LC surface. A depression is imposed at the nematic surface for each AuNP domain of depth varying between 20 and 100 nm. We can now ask the reverse question: if and how are the AuNPs themselves affected by the presence of the nematic film below? We have thus studied PSNLC films with AuNPs by SEM (Figure 4) on a slightly more concentrated area than the one studied by AFM. The AuNP domains (in white in Figure 4) are indeed more interconnected than in Figure 3. In contrast with AFM measurements, a zoom on the islands (Figure 4a–c) easily displays the AuNP structure associated with the formation of hexagonal networks. Surprisingly, we observed a very well-organized monolayer on the nematic film, characterized by a hexagonal organization similar to the one that can be obtained on a hard substrate (Supporting Information Figure S2 for comparison). The strong contrast associated with the AuNPs is consistent with the absence of nematic LC above the AuNPs, indeed already suggested by AFM results.

Localized Surface Plasmon Extinction. In order to understand if the AuNP organization is similar to that on a hard substrate, we have compared the localized surface plasmon (LSP) extinction of AuNPs directly deposited on top of the rubbed PVA substrate with that of the AuNPs organized in domains at the PSNLC surface (Figure 5). Figure 5 shows that for both systems, a large red shift of the LSP resonance wavelength is observed with respect to isolated AuNPs in solution (Supporting Information Figure S3). A similar red shift is measured with NLC films with AuNPs (Supporting Information Figure S4). This shift reflects the electromagnetic coupling between NPs that occurs when they are packed within a hexagonal lattice. We have measured the LSP extinction for incident light parallel and perpendicular to the rubbing of PVA. Consistent with the symmetry of the hexagonal packing, we find no difference in the measurements and thus we only show non-polarized data in Figure 5.

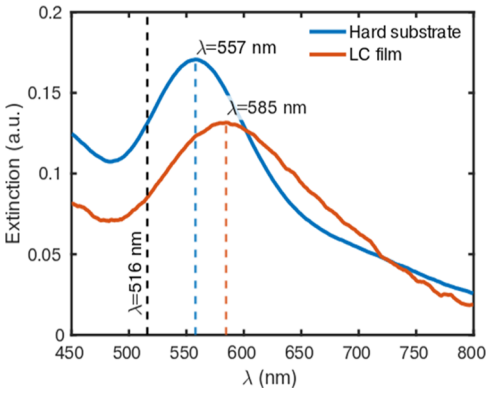

Figure 5. LSP extinction of AuNPs on a hard substrate (rubbed PVA) in blue and on a PSNLC film in red. The maximum of each extinction curve is denoted by dashed lines. The LSP resonance of a AuNP toluene solution is indicated by the dashed black line.

A striking difference between the two data sets in Figure 5 is that the red shift is significantly larger on top of the nematic film (69 nm) as compared to the case on the hard substrate without the LC (41 nm). It is known that for these NPs covered by ligands, the optical index responsible for the LSP resonance wavelength is mostly imposed by the ligands.[20,38] Thus, the fact that $n_e = 1.735$ is significantly larger than the optical index of PVA ($n = 1.5$) compared to $n_o = 1.537$ is not at the origin of the observed larger red shift for AuNPs at the NLC surface. This is indeed confirmed by the observation that the LSP resonance does not depend on the polarization of the incident light. The difference of red shift shown in Figure 5 thus leads to the following conclusion: On top of the nematic film, there is an LC-induced shortening of the inter-NP distance, in other words a shortening of the period of the hexagonal network shown on Figure 4c with respect to that on a hard substrate without LC (Supporting Information Figure S2).

DISCUSSION

When the AuNP in toluene solution droplet is deposited on the nematic, there is an almost complete dissolution of the nematic film. As the toluene evaporates, the nematic film reforms, leading to the AuNP localization at the air interface. This suggests that in the absence of topological defects in the LC film, localization of AuNPs at the LC film surface may be the equilibrium state of the composite nematic film-AuNPs. Similar observations have been obtained for cholesteric films formed in the presence of platinum or gold nanoparticles[21,23] but, in this latter case, competing with formation of aggregates in the bulk.[22] Neither, in the NLC nor in the PSNLC film are aggregates formed. This could be related to the preparation of the composites via the deposition of a droplet at the surface that may favor localization at the air interface. In comparison with the cholesteric film, there is no modulation on the nematic surface. As a result, no stripes of AuNPs are observed.[21,23] Instead, the AuNPs organize in a process that looks similar to the one leading to the well-known organization on top of a solid substrate after solvent evaporation (Supporting Information Figure S2). The filaments made of islands of ordered hexagonal AuNP networks revealed by combined POM, AFM, and SEM may be connected to the end of solvent evaporation at the LC film surface. The islands are the signature of the last solvent droplets that bring AuNPs close to each other before full solvent evaporation. The observed NP organization is the usual result of inter-AuNP van der Waals interactions that favor hexagonal organization of nanospheres. However, spectrophotometric data demonstrate that on PSNLC (Figure 5) and on NLC (Supporting Information Figure S4), the period of the hexagonal network is shortened with respect to the one on a hard, rubbed PVA surface (without a LC). This suggests that an additional

https://doi.org/10.1021/acsanm.1c00680
ACS Appl. Nano Mater. 2021, 4, 6700–6708

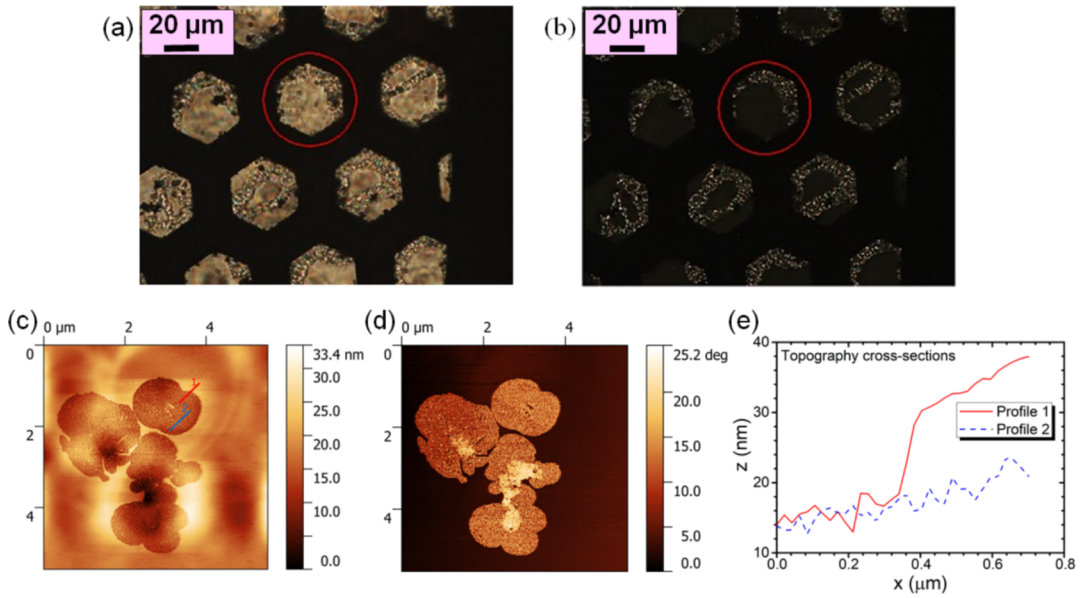

Figure 6. Optical microscopy images: (a) in transmission with a parallel polarizer, revealing the presence of the LC film within the TEM copper grid, (b) with crossed polarizers, revealing a change of birefringence from homeotropic to tilted below the NPs. (c) AFM topographical and (d) phase data for a region with AuNP domains on a 8CB smectic-A LC. (e) Corresponding topographical cross sections according to the lines drawn in (c). AuNP regions are visible in the phase data by the variations of interaction with the AFM tip, which coincide with the hole areas observed in (c). The depth of the hole that the nanoparticles dig is around 15 nm with respect to the smectic surface at the hole edge.

interaction takes place together with the inter-NP van der Waals interactions. The inter-NP spacing in the hexagonal network has been measured on the rubbed PVA surface (without a LC) by combined spectrophotometric measurements and synchrotron grazing incidence X-ray scattering (GISAXS). It is equal to 1.9 nm.[20,39−41] If we analyze the red shift of the plasmonic absorption of Figure 5 using the dipolar approximation (see "Materials and Methods"), we find that the inter-NP gap decreases from 1.9 nm without LC[20,39−41] to 1.1 nm on top of PSNLC, leading to a shortening of 0.8 nm. The additional interaction thus leads to quite a large shortening of the inter-AuNP spacing that requires high distortion and interdigitation of the dodecanethiol ligands that have an extended length of 1.8 nm. The nematic material allows for the formation of a well-organized AuNP network at the surface, however with a significantly enhanced electromagnetic coupling between AuNPs, able to significantly modify their optical properties. It is important to understand the origin of such shortening of lattice spacing. It may be related to the formation of the depression in the LC film below the AuNP domains. Since the observed shortening of the AuNP lattice spacing occurs independently of the polymerization in the nematic material (we find a similar red shift for plasmonic resonance with and without polymerization), this would imply that polymerization is not directly responsible for the establishment of the depressions. In order to check it and to understand the origin of the observed depressions, we have studied AuNP aggregation on smectic films without polymers.

Although it is very difficult to obtain reliable SEM or AFM pictures using nematic films without polymers, it is nonetheless possible to perform AFM measurements on smectic films.[42] We prepared 8CB smectic films within TEM copper grids, inducing a homeotropic texture (see "Materials and Methods"), thus avoiding distortion and the creation of defects.[28] After deposition of the same AuNP droplets on top of the smectic films, a similar anchoring modification of 8CB induced by the AuNPs is observed as revealed by POM (Figure 6a,b). Moreover, we observe the same localization of AuNPs at the 8CB surface, leading to the formation of similar depressions, as revealed by AFM measurements (Figure 6c−e). These results obtained with smectic films without polymerization confirm that polymerization in PSNLC, even if it impacts the depth of the depression, is not directly responsible for the formation of these domains at the LC surface or for the formation of depression below AuNP domains at the surface of nematic or smectic films. They also suggest that the domains could correspond to the real equilibrium state of the composite nematic/smectic film-AuNPs, in agreement with the observations that the smectic films with AuNP domains at the surface remain unchanged several months after their preparation. Finally, the fact that similar depression features below the AuNPs are observed in smectic and nematic films suggests that the origin of the depressions below AuNPs is similar in both phases. In the smectic phase, the depressions can be viewed as the result of the tilted anchoring imposed below the AuNP domains: to allow for tilted anchoring and flat smectic layers, parallel to a flat interface, a (local) transition from a smectic-A phase to a smectic-C phase is necessary. However, along with the tilt comes layer compression, as in the smectic-A to smectic-C transition. The accommodation of compressed smectic-C layers and neighboring non-compressed smectic-A ones thus creates a depression below the AuNP domains (see scheme of Figure 7). For an anchoring tilt of θ below AuNP domains and a depression depth of about h = 15 nm corresponding to the one observed in Figure 6, the number of smectic layers involved in the smectic-C/smectic-A transition is larger than $N = (h + 6)/\{P^*[1 - \cos(\theta)]\}$, 6 nm being the NP diameter and P = 3.16 nm being the smectic-A period of 8CB. This leads to between 29 and 152 smectic layers involved in the smectic-C/smectic-A transition for an anchoring tilt of 39° and 17°, respectively.

https://doi.org/10.1021/acsanm.1c00680
ACS Appl. Nano Mater. 2021, 4, 6700−6708

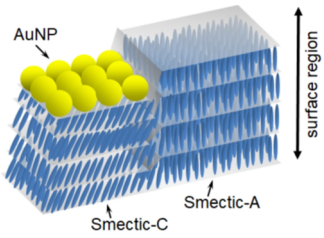

Figure 7. Schematic presentation of the depression occurring below AuNP domains due to a local smectic-C (below AuNP domain)/smectic-A (below air) transition.

How does this bear on our nematic data for 5CB? It has been observed in both experiment and modeling that nematics can display surface "freezing" and form several layers of the smectic phase near a homeotropic surface.[43,44] Since merely changing the anchoring condition from homeotropic to a tilt whose value ranges between 17° and 39° could not modify the nematic density, we postulate that a surface smectic-A phase forms and that, upon contact with the AuNPs, becomes a smectic-C. By analogy with the true equilibrium smectic of 8CB, this should lead to the formation of a depression below AuNP domains. If we postulate that the polymerization has no influence on the depression feature, then the observed depression depth of 82 nm (the average value associated with more than 100 measurements) requires the number of smectic-A/smectic-C layers to be very large, ranging from around 130 to 670, as shown by the N values obtained for an anchoring tilt of 39° and 17°, respectively, taking the 5CB smectic-A layer size close to the surface to be 2.6 nm.[35] This number is definitely too large when compared to previous results, suggesting that 5CB has a short-range smectic order with at most three to four layers near the air interface.[43,44] This leads us to conclude that the polymerization must contribute to the observed large depression depth in PSNLC with AuNP monolayers. For instance, cybotactic clusters of polymers may co-organize with 5CB into layers close to the interface, with the polymer orientation being imposed by 5CB, thus inducing an increased layer size.[45] The increased size of the polymer-stabilized smectic layers would induce a large depth of the depressions below the AuNP domains. The polymerization may also favor the surface "freezing" of the nematic structure into a smectic as previously shown in ref 45, leading to a large number of polymer-stabilized smectic layers close to the interface. Such a phenomenon may be enhanced by the directional UV-irradiation, leading to the well-known favored polymerization close to the air−AuNP interface.[46]

The smectic-C structure induced by the tilted anchoring below AuNP domains incurs an energy penalty. To decrease this energy as much as possible, the area of the AuNP domains will shrink, leading to the observed shortening of the lattice spacing. We can compare this shortening to prior work on AuNPs trapped in smectic topological defects. For small AuNPs of diameter D = 4 nm with the same dodecanthiol ligands (with a size smaller than the core of the defects), no shortening is observed.[47] The AuNPs used here, of diameter D = 6 nm, have also been embedded in 2D smectic topological defects.[20,39] There, the 2D confinement induces formation of hexagonal networks similar to the one observed at the 5CB surface but instead embedded within the 2D defects. Shortening is also observed, suggesting that these AuNPs are larger than the defect core size in contrast with AuNPs of diameter D = 4 nm. The shortening is only 0.6 nm; of the same order yet smaller than that observed here on 5CB (with both PSNLC and NLC films). In the former case, the advantage of being embedded within a topological defect core may be responsible for the smaller shortening. This however shows that the disorder induced by the AuNPs outside the topological defect core has an energy per unit area of the same order of magnitude as the one associated with the putative smectic-C/smectic-A induced by the AuNPs.

These results finally show that the LC anchoring modifications induced by the AuNP domains allow the manipulation of the AuNP domain lattice spacing and the enhancement of the coupling between AuNPs. For metallic NPs, this induces a significant red shift of the plasmonic resonance known to be associated with an enhanced electromagnetic field between neighboring NPs under light irradiation. It will be particularly appropriate to use these composite surfaces as surface-enhanced Raman scattering (SERS) surfaces for sensing applications. This effect could even be monitored using different ligands around AuNPs to further modify the LC anchoring below the AuNP domains and thus still enhance the coupling between NPs. It will be also interesting to study the possible activation of plasmonic resonance as a function of temperature, the temperature being increased above the nematic/isotropic transition (35.2 °C for 5CB) where the LC anchoring phenomenon is lost. Increase of temperature above the transition may eliminate the lattice spacing shortening. Temperature may thus become an external activator for control of the coupling between NPs in ordered NP networks when they are formed on top of nematic or smectic surfaces.

CONCLUSIONS

In conclusion, we have shown that nematic films can serve as substrates for the formation of well-ordered hexagonal monolayers of gold nanoparticles (AuNPs) of diameter D = 6 nm. This has been shown by combining optical microscopy on polymer-stabilized 5CB (PSNLC) and pure 5CB (NLC) films, AFM and SEM on PSNLC films, and spectrophotometry on PSNLC films and NLC films. The same features have been shown on smectic surfaces by combining optical microscopy and AFM. However, we also show how both AuNP networks and nematic films are mutually impacted by each other. The AuNP network period is shortened by the surrounding nematic film and depressions are created at the nematic surface, where the AuNP domains are formed. We show that it is related to a tilt of the nematic anchoring induced below the AuNP monolayers, ranging from 17° to 39°. In the smectic film, the anchoring tilt transforms smectic-A layers into smectic-C layers. Depressions through layer shrinkage may then become necessary to accommodate the neighboring smectic-A (without AuNPs) and smectic-C (with AuNP monolayers) areas. The same phenomenon occurs with nematic films in relation with the known surface-induced smectic-A structure of the nematic film at the interface transformed into a smectic-C one. The shortening of the AuNP network period may be induced by the necessary minimization of the surface of the smectic-C areas in relation to the energy cost of the local smectic-A/smectic-C transition. We find that when the nematic film is polymer-stabilized, the depression depth is increased either due to an increased smectic layer size or to an increased number of polymer-stabilized smectic layers close to the surface with respect to NLC films. These results not only open the route for

https://doi.org/10.1021/acsanm.1c00680
ACS Appl. Nano Mater. 2021, 4, 6700−6708

a control of the coupling between NPs at the LC surface through the use of various ligands around NPs that would modify the LC anchoring underneath the AuNP domains, but also for activated control through temperature changes reaching the nematic/smectic transition temperature.

■ ASSOCIATED CONTENT

Supporting Information

The Supporting Information is available free of charge at https://pubs.acs.org/doi/10.1021/acsanm.1c00680.

Optical microscopy image of a nematic liquid crystal film in the presence of AuNPs, SEM image of self-organized AuNPs on unidirectionally rubbed PVA on a silicon substrate, and LSP extinction of isolated AuNPs suspended in toluene and of AuNPs on a nematic film (PDF)

■ AUTHOR INFORMATION

Corresponding Author

Emmanuelle Lacaze − *Sorbonne Université, CNRS, Institut des Nanosciences de Paris, INSP, Paris F-75005, France*; Email: emmanuelle.lacaze@insp.jussieu.fr

Authors

Ines Gharbi − *Sorbonne Université, CNRS, Institut des Nanosciences de Paris, INSP, Paris F-75005, France; Faculté des Sciences de Tunis, LR99ES16 Physique de la Matière Molle et de la Modélisation Electromagnétique, Université de Tunis El Manar, Tunis 2092, Tunisie;* orcid.org/0000-0002-5872-9131

Viviana Palacio-Betancur − *Pritzker School of for Molecular Engineering, University of Chicago, Chicago 60637, Illinois, United States;* orcid.org/0000-0002-1588-318X

Habib Ayeb − *Faculté des Sciences de Tunis, LR99ES16 Physique de la Matière Molle et de la Modélisation Electromagnétique, Université de Tunis El Manar, Tunis 2092, Tunisie*

Dominique Demaille − *Sorbonne Université, CNRS, Institut des Nanosciences de Paris, INSP, Paris F-75005, France*

Juan J. de Pablo − *Pritzker School of for Molecular Engineering, University of Chicago, Chicago 60637, Illinois, United States; Materials Science Division, Argonne National Laboratory, Lemont 60439, Illinois, United States;* orcid.org/0000-0002-3526-516X

Randall D. Kamien − *Department of Physics and Astronomy, University of Pennsylvania, Philadelphia 19104, Pennsylvania, United States*

Complete contact information is available at: https://pubs.acs.org/10.1021/acsanm.1c00680

Notes

The authors declare no competing financial interest.

■ ACKNOWLEDGMENTS

We would like to thank Abdelhafidh Gharbi for precious comments and fruitful discussions, Christophe Blanc for useful help with the polymerization test, and Denis Limagne for technical support. I.G. was supported by the Tunisian Ministry for Higher Education, Research, and Technology and by the CNRS-UMR7588. I.G.'s travel between Tunis and Paris was supported by a grant from Université de Tunis El Manar and more specifically from LR99ES16. V.P.-B. is thankful to the Fulbright commission in Colombia and Colciencias, as well as the Chateaubriand Fellowship program and the Eiffel Excellence Scholarship program. R.D.K. was supported by NSF MRSEC grant DMR-1720530 and by a Simons Investigator Grant from the Simons Foundation. J.J.dP. is supported by NSF MRSEC grant DMR-2011854.We are grateful to Brigitte Pansu for providing Au nanoparticles and thank Soleil synchrotron and Doru Constantin for the measurement of the diameter and polydispersity in the size of AuNPs using SAXS on the beamline Swing.

■ REFERENCES

(1) Blanc, C.; Coursault, D.; Lacaze, E. Ordering Nano- and Microparticles Assemblies with Liquid Crystals. *Liq. Cryst. Rev.* **2013**, *1*, 83−109.

(2) Lagerwall, J. P. F.; Scalia, G. *Liquid Crystals with Nano and Microparticles*; World Scientific Publishing Company, 2017, Vol. *26* (4), pp 126−127.

(3) Choudhary, A.; Singh, G.; Biradar, A. M. Advances in Gold Nanoparticle−Liquid Crystal Composites. *Nanoscale* **2014**, *6*, 7743−7756.

(4) Sridevi, S.; Prasad, S. K.; Nair, G. G.; D'Britto, V.; Prasad, B. L. V. Enhancement of Anisotropic Conductivity, Elastic, and Dielectric Constants in a Liquid Crystal-Gold Nanorod System. *Appl. Phys. Lett.* **2010**, *97*, 151913.

(5) Mishra, M.; Kumar, S.; Dhar, R. Effect of Dispersed Colloidal Gold Nanoparticles on the Electrical Properties of a Columnar Discotic Liquid Crystal. *RSC Adv.* **2014**, *4*, 62404−62412.

(6) Tomašovičová, N.; Timko, M.; Mitróová, Z.; Koneracká, M.; Rajňak, M.; Éber, N.; Tóth-Katona, T.; Chaud, X.; Jadzyn, J.; Kopčanský, P. Capacitance Changes in Ferronematic Liquid Crystals Induced by Low Magnetic Fields. *Phys. Rev. E: Stat., Nonlinear, Soft Matter Phys.* **2013**, *87*, 014501.

(7) Mishra, R.; Hazarika, J.; Hazarika, A.; Gogoi, B.; Dubey, R.; Bhattacharjee, D.; Singh, K. N.; Alapati, P. R. Dielectric Properties of a Strongly Polar Nematic Liquid Crystal Compound Doped with Gold Nanoparticles. *Liq. Cryst.* **2018**, *45*, 1661−1671.

(8) Lee, E.; Xia, Y.; Ferrier, R. C.; Kim, H.-N.; Gharbi, M. A.; Stebe, K. J.; Kamien, R. D.; Composto, R. J.; Yang, S. Fine Golden Rings: Tunable Surface Plasmon Resonance from Assembled Nanorods in Topological Defects of Liquid Crystals. *Adv. Mater.* **2016**, *28*, 2731−2736.

(9) Qi, H.; Hegmann, T. Formation of Periodic Stripe Patterns in Nematic Liquid Crystals Doped with Functionalized Gold Nanoparticles. *J. Mater. Chem.* **2006**, *16*, 4197−4205.

(10) Qi, H.; Kinkead, B.; Marx, V. M.; Zhang, H. R.; Hegmann, T. Miscibility and Alignment Effects of Mixed Monolayer Cyanobiphenyl Liquid-Crystal-Capped Gold Nanoparticles in Nematic Cyanobiphenyl Liquid Crystal Hosts. *ChemPhysChem* **2009**, *10*, 1211−1218.

(11) Yoshida, H.; Tanaka, Y.; Kawamoto, K.; Kubo, H.; Tsuda, T.; Fujii, A.; Kuwabata, S.; Kikuchi, H.; Ozaki, M. Nanoparticle-Stabilized Cholesteric Blue Phases. *Appl. Phys. Express* **2009**, *2*, 121501.

(12) Karatairi, E.; Rožič, B.; Kutnjak, Z.; Tzitzios, V.; Nounesis, G.; Cordoyiannis, G.; Thoen, J.; Glorieux, C.; Kralj, S. Nanoparticle-Induced Widening of the Temperature Range of Liquid-Crystalline Blue Phases. *Phys. Rev. E: Stat., Nonlinear, Soft Matter Phys.* **2010**, *81*, 041703.

(13) Rožič, B.; Tzitzios, V.; Karatairi, E.; Tkalec, U.; Nounesis, G.; Kutnjak, Z.; Cordoyiannis, G.; Rosso, R.; Virga, E. G.; Muševič, I.; Kralj, S. Theoretical and Experimental Study of the Nanoparticle-Driven Blue Phase Stabilisation. *Eur. Phys. J. E* **2011**, *34*, 17.

(14) Senyuk, B.; Evans, J. S.; Ackerman, P. J.; Lee, T.; Manna, P.; Vigderman, L.; Zubarev, E. R.; van de Lagemaat, J.; Smalyukh, I. I. Shape-Dependent Oriented Trapping and Scaffolding of Plasmonic Nanoparticles by Topological Defects for Self-Assembly of Colloidal Dimers in Liquid Crystals. *Nano Lett.* **2012**, *12*, 955−963.

(15) Cordoyiannis, G.; Rao Jampani, V. S.; Kralj, S.; Dhara, S.; Tzitzios, V.; Basina, G.; Nounesis, G.; Kutnjak, Z.; Pati Tripathi, C. S.; Losada-Pérez, P.; Jesenek, D.; Glorieux, C.; Muševič, I.; Zidanšek, A.; Ameinitsch, H.; Thoen, J. Different Modulated Structures of Topological Defects Stabilized by Adaptive Targeting Nanoparticles. *Soft Matter* **2013**, *9*, 3956−3964.
(16) Evans, J. S.; Ackerman, P. J.; Broer, D. J.; Lagemaat, J.; Smalyukh, I. I. Optical Generation, Templating, and Polymerization of Three-Dimensional Arrays of Liquid-Crystal Defects Decorated by Plasmonic Nanoparticles. *Phys. Rev. E: Stat., Nonlinear, Soft Matter Phys.* **2013**, *87*, 032503.
(17) Gharbi, M. A.; Manet, S.; Lhermitte, J.; Brown, S.; Milette, J.; Toader, V.; Sutton, M.; Reven, L. Reversible Nanoparticle Cubic Lattices in Blue Phase Liquid Crystals. *ACS Nano* **2016**, *10*, 3410−3415.
(18) Rožič, B.; Fresnais, J.; Molinaro, C.; Calixte, J.; Umadevi, S.; Lau-Truong, S.; Felidj, N.; Kraus, T.; Charra, F.; Dupuis, V.; Hegmann, T.; Fiorini-Debuisschert, C.; Gallas, B.; Lacaze, E. Oriented Gold Nanorods and Gold Nanorod Chains within Smectic Liquid Crystal Topological Defects. *ACS Nano* **2017**, *11*, 6728−6738.
(19) Mundoor, H.; Sheetah, G. H.; Park, S.; Ackerman, P. J.; Smalyukh, I. I.; van de Lagemaat, J. Tuning and Switching a Plasmonic Quantum Dot "Sandwich" in a Nematic Line Defect. *ACS Nano* **2018**, *12*, 2580−2590.
(20) Do, S.-P.; Missaoui, A.; Coati, A.; Resta, A.; Goubet, N.; Royer, S.; Guida, G.; Briand, E.; Lhuillier, E.; Garreau, Y.; Babonneau, D.; Goldmann, M.; Constantin, D.; Croset, B.; Gallas, B.; Lacaze, E. Interactions Between Topological Defects and Nanoparticles. *Front. Phys.* **2020**, *7*, 234.
(21) Mitov, M.; Portet, C.; Bourgerette, C.; Snoeck, E.; Verelst, M. Long-Range Structuring of Nanoparticles by Mimicry of a Cholesteric Liquid Crystal. *Nat. Mater.* **2002**, *1*, 229−231.
(22) Mitov, M.; Bourgerette, C.; Guerville, F. Fingerprint Patterning of Solid Nanoparticles Embedded in a Cholesteric Liquid Crystal. *J. Phys.: Condens. Matter* **2004**, *16*, S1981−S1988.
(23) Bitar, R.; Agez, G.; Mitov, M. Cholesteric Liquid Crystal Self-Organization of Gold Nanoparticles. *Soft Matter* **2011**, *7*, 8198−8206.
(24) Tran, L.; Kim, H.-N.; Li, N.; Yang, S.; Stebe, K. J.; Kamien, R. D.; Haase, M. F. Shaping Nanoparticle Fingerprints at the Interface of Cholesteric Droplets. *Sci. Adv.* **2018**, *4*, No. eaat8597.
(25) Peng, S.; Lee, Y.; Wang, C.; Yin, H.; Dai, S.; Sun, S. A Facile Synthesis of Monodisperse Au Nanoparticles and Their Catalysis of CO Oxidation. *Nano Res.* **2008**, *1*, 229−234.
(26) Dierking, I. Polymer Network−Stabilized Liquid Crystals. *Adv. Mater.* **2000**, *12*, 167−181.
(27) Gharbi, I.; Missaoui, A.; Demaille, D.; Lacaze, E.; Rosenblatt, C. Persistence of Smectic-A Oily Streaks into the Nematic Phase by UV Irradiation of Reactive Mesogens. *Crystals* **2017**, *7*, 358.
(28) Brake, J. M.; Abbott, N. L. An Experimental System for Imaging the Reversible Adsorption of Amphiphiles at Aqueous−Liquid Crystal Interfaces. *Langmuir* **2002**, *18*, 6101−6109.
(29) Kreibig, U.; Vollmer, M. *Optical properties of metal clusters*; Springer Berlin Heidelberg, 2013.
(30) Topping, J.; Chapman, S. On the Mutual Potential Energy of a Plane Network of Doublets. *Proc. R. Soc. Lond.—Ser. A Contain. Pap. a Math. Phys. Character* **1927**, *114*, 67−72.
(31) van der Hoff, B. M. E.; Benson, G. C. A Method for the Evaluation of Some Lattice Sums Occurring in Calculations of Physical Properties of Crystals. *Can. J. Phys.* **1953**, *31*, 1087−1094.
(32) Johnson, P. B.; Christy, R. W. Optical Constants of the Noble Metals. *Phys. Rev. B* **1972**, *6*, 4370−4379.
(33) Garcia, M. A.; de la Venta, J.; Crespo, P.; LLopis, J.; Penadés, S.; Fernández, A.; Hernando, A. Surface Plasmon Resonance of Capped Au Nanoparticles. *Phys. Rev. B: Condens. Matter Mater. Phys.* **2005**, *72*, 241403.
(34) Miller, D. S.; Carlton, R. J.; Mushenheim, P. C.; Abbott, N. L. Introduction to Optical Methods for Characterizing Liquid Crystals at Interfaces. *Langmuir* **2013**, *29*, 3154−3169.
(35) Lelidis, I.; Gharbi, A.; Durand, G. A New Optical Method to Measure Angular Tilts for Planar Anchored Nematic Liquid Crystals. *Mol. Cryst. Liq. Cryst. Sci. Technol., Sect. A* **1992**, *223*, 263−276.
(36) Mohammadimasoudi, M.; Neyts, K.; Beeckman, J.. Thin Film Polarizer and Color Filter Based on Photo-Polymerizable Nematic Liquid Crystal. *Emerging Liquid Crystal Technologies X*; International Society for Optics and Photonics, 2015; Vol. *9384*, p 93840E.
(37) Drawhorn, R. A.; Abbott, N. L. Anchoring of Nematic Liquid Crystals on Self-Assembled Monolayers Formed from Alkanethiols on Semitransparent Films of Gold. *J. Phys. Chem.* **1995**, *99*, 16511−16515.
(38) Mulvaney, P. Surface Plasmon Spectroscopy of Nanosized Metal Particles. *Langmuir* **1996**, *12*, 788−800.
(39) Do, S.-P.; Missaoui, A.; Coati, A.; Coursault, D.; Jeridi, H.; Resta, A.; Goubet, N.; Wojcik, M. M.; Choux, A.; Royer, S.; Briand, E.; Donnio, B.; Gallani, J. L.; Pansu, B.; Lhuillier, E.; Garreau, Y.; Babonneau, D.; Goldmann, M.; Constantin, D.; Gallas, B.; Croset, B.; Lacaze, E. From Chains to Monolayers: Nanoparticle Assembly Driven by Smectic Topological Defects. *Nano Lett.* **2020**, *20*, 1598−1606.
(40) Goubet, N.; Richardi, J.; Albouy, P.-A.; Pileni, M.-P. Which Forces Control Supracrystal Nucleation in Organic Media? *Adv. Funct. Mater.* **2011**, *21*, 2693−2704.
(41) Gauvin, M.; Wan, Y.; Arfaoui, I.; Pileni, M.-P. Mechanical Properties of Au Supracrystals Tuned by Flexible Ligand Interactions. *J. Phys. Chem. C* **2014**, *118*, 5005−5012.
(42) Michel, J.-P.; Lacaze, E.; Alba, M.; De Boissieu, M.; Gailhanou, M.; Goldmann, M. Optical Gratings Formed in Thin Smectic Films Frustrated on a Single Crystalline Substrate. *Phys. Rev. E: Stat., Nonlinear, Soft Matter Phys.* **2004**, *70*, 011709.
(43) Fukuto, M.; Gang, O.; Alvine, K. J.; Ocko, B. M.; Pershan, P. S. Wetting of Liquid-Crystal Surfaces and Induced Smectic Layering at a Nematic-Liquid Interface: An x-Ray Reflectivity Study. *Phys. Rev. E: Stat., Nonlinear, Soft Matter Phys.* **2008**, *77*, 031607.
(44) Sadati, M.; Ramezani-Dakhel, H.; Bu, W.; Sevgen, E.; Liang, Z.; Erol, C.; Rahimi, M.; Taheri Qazvini, N.; Lin, B.; Abbott, N. L.; Roux, B.; Schlossman, M. L.; de Pablo, J. J. Molecular Structure of Canonical Liquid Crystal Interfaces. *J. Am. Chem. Soc.* **2017**, *139*, 3841−3850.
(45) Noh, J.; Henx, B.; Lagerwall, J. P. F. Taming Liquid Crystal Self-Assembly: The Multifaceted Response of Nematic and Smectic Shells to Polymerization. *Adv. Mater.* **2016**, *28*, 10170−10174.
(46) Kamal, T.; Park, S.-Y. A Liquid Crystal Polymer Based Single Layer Chemo-Responsive Actuator. *Chem. Commun.* **2014**, *50*, 2030−2033.
(47) Coursault, D.; Blach, J.-F.; Grand, J.; Coati, A.; Vlad, A.; Zappone, B.; Babonneau, D.; Lévi, G.; Félidj, N.; Donnio, B.; Gallani, J.-L.; Alba, M.; Garreau, Y.; Borensztein, Y.; Goldmann, M.; Lacaze, E. Tailoring Anisotropic Interactions between Soft Nanospheres Using Dense Arrays of Smectic Liquid Crystal Edge Dislocations. *ACS Nano* **2015**, *9*, 11678−11689.

https://doi.org/10.1021/acsanm.1c00680
ACS Appl. Nano Mater. 2021, 4, 6700−6708